

Final Laboratory Integration and Test of the Keck Interferometer Nuller

S.L. Crawford, M. M. Colavita, J. I. Garcia, E. R. Ligon, B. Mennesson,
C. G. Paine, E. Serabyn, R. F. Smythe, M. R. Swain, and G. Vasisht
Jet Propulsion Laboratory, California Institute of Technology,
4800 Oak Grove Dr., Pasadena, CA 91109 USA

ABSTRACT

Mid-infrared (8-13 μ m) nulling is a key observing mode planned for the NASA-funded Keck Interferometer at the Keck Observatory on the summit of Mauna Kea in Hawaii. By destructively interfering and thereby canceling the on-axis light from nearby stars, this observing mode will enable the characterization of the faint emission from exo-zodiacal dust surrounding these stellar systems. We report here the null leakage error budget and pre-ship results obtained in the laboratory after integration of the nulling beam combiner with its mid-infrared camera and key components of the Keck Interferometer. The mid-infrared nuller utilizes a dual-polarization, modified Mach-Zehnder (MMZ) beam combiner in conjunction with an atmospheric dispersion corrector to achieve broadband achromatic nulling.

Keywords: nulling, stellar interferometer, starlight suppression, extrasolar planet detection

1. INTRODUCTION

The long term goal of NASA's Origins program is to discover life beyond the immediate confines of the earth and beyond our solar system. A major step toward this goal would be the ability to directly detect or image extrasolar planets capable of harboring life as we know it. Although we are decades away from having the technical capability to image earth-like extrasolar planets, nascent efforts are under way to bridge that formidable technological divide while addressing some fundamental astrophysical questions.

One of the questions which astronomers would like to answer in the near-term is whether the distribution of zodiacal dust in our own solar system is typical of other systems likely to have terrestrial planets. The mid-infrared is the most favorable wavelength region for detecting extrasolar planets since the brightness contrast between the parent star and its planets is smaller than in other observing spectral bandpasses. However, the emission from any dust in the plane of these planets (i.e., the exo-zodiacal light) is also prominent in the infrared and thus would tend to obscure potential planetary signatures. Thus, one goal of the Keck Interferometer is to find target systems in which the quantity of dust is not so large as to impede extrasolar planet searches by future space-based arrays such as the Terrestrial Planet Finder¹ and DARWIN².

The Keck Interferometer nuller is designed to conduct this potential target search by nulling or canceling out most of the infrared emission from a star in order to reveal the far dimmer emission from any exo-zodiacal dust surrounding it. Using the projected 85-m baseline of the two Keck telescopes, the nominal performance of the nuller should allow it to detect the exo-zodiacal light from a Sun-like star at a distance of 10 parsecs down to a level of 10 times the infrared emission of zodiacal light in our own solar system after three hours of source integration. For a class G2 star at 10 pc, the baseline-limited null depth at $\lambda = 10 \mu\text{m}$, with a baseline of 85 m, is expected to be 10^{-3} .

Earlier, we reported results for the intrinsic performance of the nuller instrument at an inverse null depth of 7500 for a 3- μm wide bandpass in the mid-infrared for a broadband thermal source³. This performance evaluation has now been extended to include integration and testing with spare key components of the Keck Interferometer at JPL rather than on the summit of Mauna Kea. In particular, the integration and test (I&T) setup (Figure 1) consisted of a 2- μm fringe tracker, a bank of four fixed and four active delay line carts, and a metrology system for monitoring pathlength fluctuations. For the first time, we also integrated the nuller with its mid-infrared camera which had been undergoing concurrent development.

Figure 1. Optical schematic of the nuller integration and test setup (view from northwest).

2. OPTICAL LAYOUT

To simulate a stellar source, a source plate (Figs. 2 and 3) injects a collimated broadband thermal stimulus (with a blackbody temperature near 1570 °K) downstream of the nuller and in the opposite direction that the stellar beams would propagate. The cross-combiner (XC) beamsplitter (BS) divides this stimulus beam between the primary and secondary nullers (Figs. 2 and 4) to produce four input beams. Once retroreflected, these four input beams will represent the four beams from the split pupils of the two 10-m Keck telescopes⁴.

Once the input beams exit the nuller breadboard, they propagate through four delay lines, reflect off K-band/N-band beamsplitters, and are retroreflected by optical flats with tip/tilt actuation (Figure 1). The K/N splitters leak enough of the K-band light to feed another bank of delay lines which propagate the beams to the 2- μm fringe tracker. Upon returning to the nuller breadboard, these four input beams will be split and recombined by the primary nuller, secondary nuller, and cross-combiner beamsplitter to yield four output beams. Each of the output beams consists of the combined beam from one of the two nulled outputs from the primary nuller and the corresponding nulled output from the secondary nuller. Finally, an actuated periscope assembly then directs all four beams into the 10- μm camera (Figure 5).

Figure 2. Scaled layout of the dual modified Mach-Zehnder nuller, source plate, and the KALI periscope/pedestal.

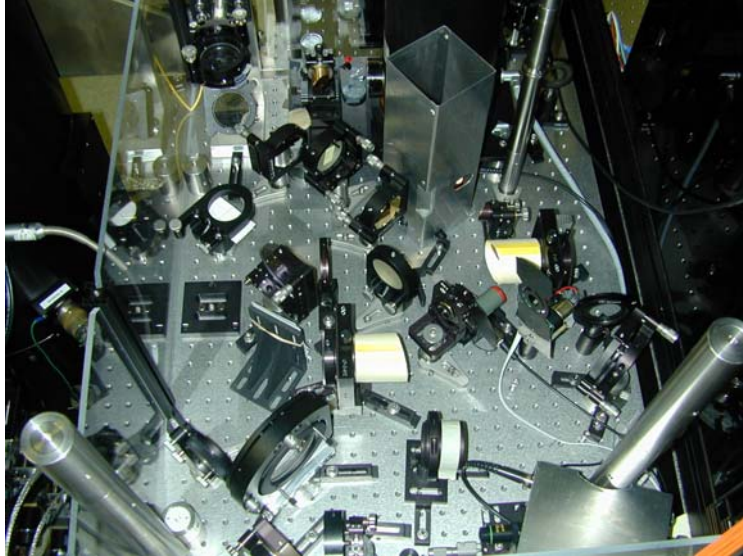


Figure 3. Keck Nuller Source Plate (view from south).

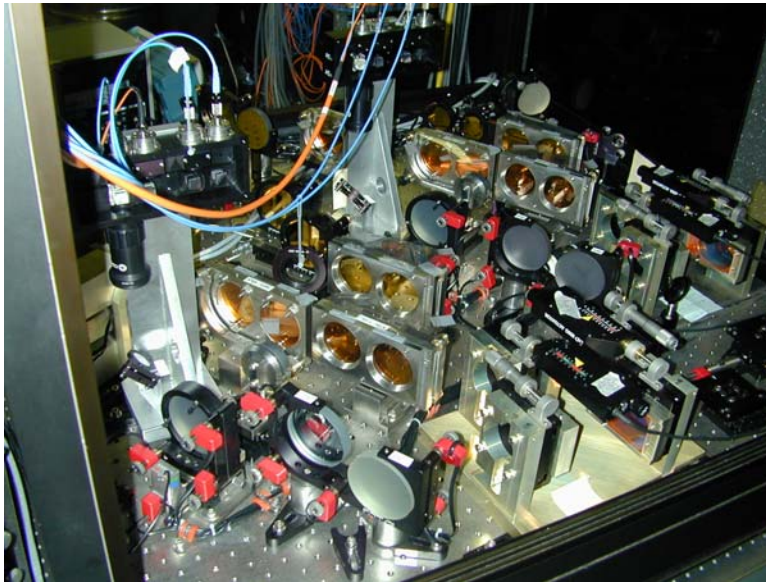


Figure 4. Dual Modified Mach-Zehnder Nuller (view from southwest).

The primary function of 10- μm camera for the Keck nuller (otherwise known as the KALI camera⁵) is to disperse the incident light onto the Boeing 128x128 pixel Si:As BIB array into several narrow spectral channels to enable tracking of the central dark fringe⁶.

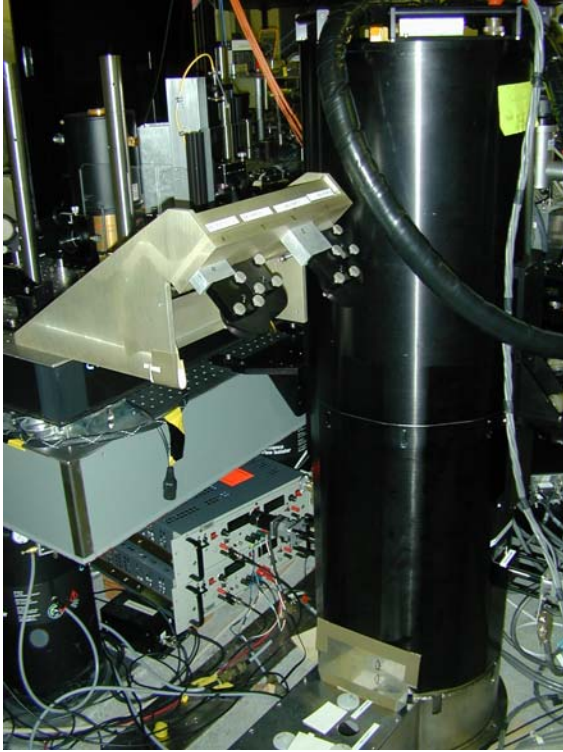


Figure 5. KALI camera dewar on its pedestal with periscope assembly (view from northwest).

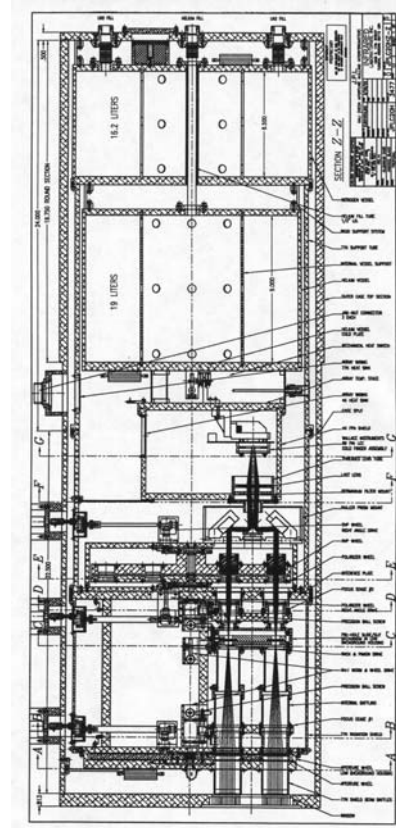


Figure 6. KALI inner optomechanics.

3. ESTIMATED PERFORMANCE

The goal of 10 zodi detectability leads to a number of challenging performance requirements for the nuller which are embodied in the null leakage error budget^{7,8,9}. These leakage terms can be categorized into additive achromatic and chromatic errors that degrade the overall null depth and can be used to estimate the system-level performance of the I&T setup. Assuming a mean wavelength $\lambda = 11 \mu\text{m}$:

<i>Achromatic Terms</i>	Estimator	Parameter	Value	Leakage	Comment
OPD (windowed)	$L = \frac{1}{4} (2\pi\sigma_{\text{OPD}}/\lambda)^2$	σ_{OPD} (nm rms)	35	0.000100	metrology reads 30-42 nm rms when tracking
Intensity balance	$L = 1/16 \Delta^2$	Δ , relative intensity difference bt arms	2.0%	0.000025	Typical value during measurements
Intensity fluctuations	$L = 1/8 \sigma_{\text{ii}}^2$	σ_{ii} , total intensity rms each arm	1.0%	0.000013	Based on observed fluctuations when at peak
Pure image rotation	$L = \frac{1}{4} (\pi\theta/180)^2$	θ , rotation (deg)	0	0.000000	Drops out in double pass (measured 0.25 deg)
Static tilt with diff-limited det. pinhole	$L_{7a} \cong 0.4 t^2$	t , total vector tilt difference (waves)	0.014	0.000083	Assume 1/4 wave HeNe step size to optimize tilt, ($t \sim 1/4 \lambda_{\text{HeNe}}/\lambda$)
Dynamic tilt with diff-limited det. pinhole	$L \cong 0.4 t^2$	t , total vector tilt difference (waves)	0.0115	0.000053	Based on IR laser measurement predicting 19,000:1
<i>induced shear from tilt @ Fresnel number F=3</i>	$s' = t/F$	t , total vector tilt difference (waves)	0.005	n/a	Compute from static tilt term; we use non-sheared output, so should be only contrib.
Static shear with diff-limited det. pinhole	$L \sim 0.4 s'^2$	s' , relative shear (frac of beam diameter)		0.000009	Approximate, by analogy with tilt
<i>induced shear from tilt @ Fresnel number F=3</i>	$s' = t/F$	t , total vector tilt difference (waves)	0.004	n/a	Compute from dynamic tilt term
Dynamic shear with diff-limited det. pinhole	$L \sim 0.4 s'^2$	s' , relative shear (frac of beam diameter)		0.000006	Approximate, by analogy with tilt

<i>Achromatic Terms</i>	Estimator	Parameter	Value	Leakage	Comment
Focus + astig X,Y w/ diff-limited det. pinhole	$L \cong 3 w^2$	w, total rms phase difference in those modes (waves)	0.006	0.000104	Assume $1/4 \lambda_{\text{HeNe}}/\lambda$ p-v for each beam for these modes. Use 0.29 p-v to rms conversion. x sqrt(2) for both beams.
Coma (4 terms) w/ diff-limited det. pinhole	$L \cong 0.8 w^2$	w, total rms phase difference in those modes (waves)	0.006	0.000028	Assume $1/4 \lambda_{\text{HeNe}}/\lambda$ p-v for each beam for these modes. Use 0.29 p-v to rms conversion. x sqrt(2) for both beams.
Amplitude curvature across pupil	$L = (1/48)*(\Delta)^2$	Δ , peak I mismatch	2.5%	0.000013	

Table 1: Achromatic leakage terms in the laboratory error budget

<i>Chromatic Terms</i>	Estimator	Parameter	Value	Leakage	Comment
Pure s-p phase shift	$L = 1/16$ $(\pi\phi/180)^2$	ϕ (deg)	3	0.000171	Upper bound. (Doesn't show up w/ (polz'd) laser). Could be smaller.
<i>induced shear from tilt @ Fresnel number F=3</i>	$s'=t/F$	s' , relative shear (frac of beam diameter)	0.005	n/a	Compute using static tilt, above, in achromatic section
Static shear for finite source pinhole	$L_{6a} = 0.6 (p's)^2$	s' , relative shear; p' , relative pinhole size (frac of λ f#)		0.000014	We use non-sheared output; induced tilt term should be only contributor (i.e., let $p' \sim 1$)
<i>induced shear from tilt @ Fresnel number F=3</i>	$s'=t/F$	s' , relative shear (frac of beam diameter)	0.004	n/a	Compute using dynamic tilt, above, in achromatic section
Dynamic shear for finite source pinhole	$L = 0.6 (p's)^2$	s' , relative shear; p' , relative pinhole size (frac of λ f#)		0.000009	We use non-sheared output; induced tilt term should be only contributor (i.e., let $p' \sim 1$)
Tilt-shear cross term for finite source pinhole	$L \cong 2(L_{6a}L_{7a})^{1/2}$	L6a - static shear leakage; L7a - static tilt leakage		0.000068	Approximate using leakage values above
<i>induced mag from defocus @ Fresnel number F=3</i>	$m'=(8/F)*e$	e , focus diff bt arms (p-v waves)	0.031	n/a	Assume 0.2 w p-v focus difference between beams at HeNe ($e \sim 0.2 \lambda_{\text{HeNe}}/\lambda$)
Pupil magnification mismatch for finite source pinhole	$L = 0.08 (m'p')^2$	m' , frac. mag. error; p' , rel pinhole size		0.000075	Induced focus term should be only contributor (i.e., let $p' \sim 1$)
<i>ADC error based on null sidelobe symmetry sym == (L-R) / 0.5(L+R)</i>	$\varepsilon = (\pi/2)_{\text{sym}}$	symmetry (%)	0.157	n/a	assume 10% sidelobe symmetry
ADC setting (e) for spectral res R[=5]	$L = (1/48)*(\varepsilon/R)^2$	ε , ADC setpoint error; GD-PD (radians phase)		0.000021	GD-PD = group delay - phase delay
Unbalanced angular dispersion with diff-limited det. pinhole	$L \cong 0.4 w^2/12$	w, rms dispersion across band (waves rms)	0.009	0.000003	measure 1' wedge; scale this based on 6' is 10,000:1
Phase curvature across the band	$L = (C/384)^2$	C, phase curvature (degrees p-v)	2.5	0.000042	Upper bound after correction
Amplitude curvature across the band	$L = (1/48)*(\Delta)^2$	Δ , peak I mismatch	2.5%	0.000013	

Table 2: Chromatic leakage terms in the laboratory error budget

The reciprocal of the sum of the above achromatic and chromatic leakage terms yields a predicted inverse null depth of 1178 (or conversely, a null depth of $8.5e^{-4}$).

4. EXPERIMENTAL RESULTS

Prior to shipment of the nuller to the summit of Mauna Kea, we verified the final lab performance of the instrument for both null depth and null depth stability. As shown in Figures 7 through 9, the null depth was measured over consecutive days and during different times of the day without any attempts to re-optimize between data sets:

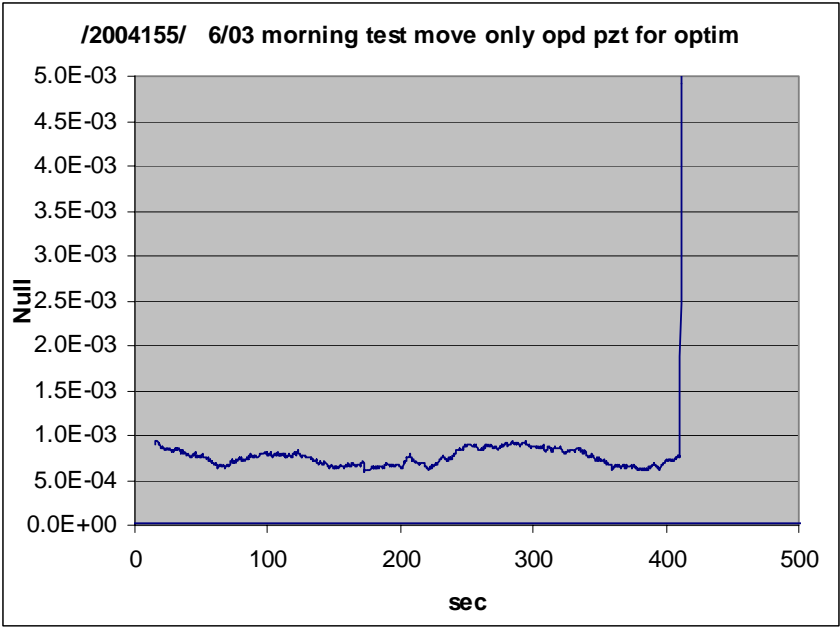


Figure 7. Null Signal (morning).

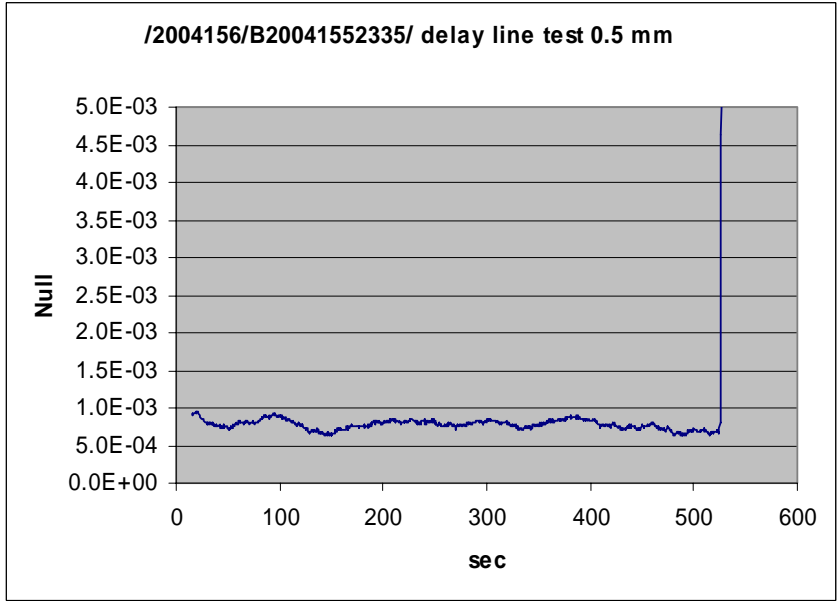


Figure 8. Null Signal (afternoon)

Figure 9. Null Signal (afternoon, following day)

Note that the measured null depths were in good agreement with the predicted performance. These results were obtained for 25-mm diameter white-light beams from a 60-micron source spectrally dispersed across an 8x3 superpixel, a 150- μ m detector pinhole, and a synthesized spectral bandpass from 10 to 12 microns (FWHM).

5. SUMMARY

The Keck Interferometer Nuller was integrated with its mid-infrared camera and other key subsystems of the Keck Interferometer in a laboratory to demonstrate stable cancellation ($> 1000:1$ over several minutes) of a broadband thermal source in the mid-infrared. The pathlength was monitored and stabilized by laser metrology and active delay lines with feed-forward from a K-band fringe tracker. With the conclusion of the integration and test phase, the nulling instrument was shipped to the Keck Observatory in June 2004 for integration with the Keck Interferometer and the initiation of on-sky engineering tests¹⁰.

ACKNOWLEDGMENTS

This work was carried out at the Jet Propulsion Laboratory, California Institute of Technology, under contract with the National Aeronautics and Space Administration.

REFERENCES

1. D. Coulter, "NASA's Terrestrial Planet Finder Mission: The Search for Habitable Planets", in Proc. Towards Other Earths: DARWIN/TPF and the Search for Extrasolar Terrestrial Planets, Heidelberg, Germany, ESA **SP-539**, p. 47 (2003).
2. A. Karlsson and L. Kaltenecker, "The Technology of DARWIN", in Proc. Towards Other Earths: DARWIN/TPF and the Search for Extrasolar Terrestrial Planets, Heidelberg, Germany, ESA **SP-539**, p. 41 (2003).
3. B. Mennesson, S. L. Crawford, E. Serabyn, et al., "Laboratory Performance of the Keck Interferometer Nulling Beam Combiner", Proceedings of the Conference on Towards Other Earths: DARWIN/TPF and the Search for Extrasolar Terrestrial Planets, Heidelberg, Germany, ESA **SP-539**, p. 525 (2003).
4. E. Serabyn, A. Booth, M.M. Colavita, et al., "The Keck Interferometer Nuller: System Architecture and Laboratory Performance", Proc. SPIE, **5491**, p. 806 (2004).

5. M.J. Creech-Eakman, J.D. Moore, D.L. Palmer, and E. Serabyn, "KALI Camera: Mid-infrared Camera for the Keck Interferometer Nuller", Proc. SPIE, **4841**, p. 330 (2003).
6. C. Koresko, B. Mennesson, E. Serabyn, et al., "Longitudinal Dispersion Control for the Keck Interferometer Nuller", Proc. SPIE, **4838**, p. 625 (2003).
7. M.M. Colavita, internal JPL memo, April 2004.
8. E. Serabyn, "Nulling Interferometry: Symmetry Requirements and Experimental Results", Proc. SPIE, **4006**, p. 328, (2000).
9. B. Mennesson, M. Ollivier, and C. Ruilier., "Use of single-mode waveguides to correct the optical defects of a nulling interferometer", JOSA **19**, p. 596 (2002).
10. E. Serabyn, E. Appleby, J. Bell, et al., "Keck Interferometer Nuller Update", Proc. SPIE, **5905**, (this conference, 2005).